High-Speed Atomic Force Microscopy Reveals Rotary Catalysis of Rotorless F_1-ATPase

Takayuki Uchihashi, *et al.*

Science **333**, 755 (2011);
DOI: 10.1126/science.1205510

prevailing impact of heterometal chemistry on the efficiency of the reaction; at the same time, the merging of the product profiles of the two nitrogenases in D_2O points to a critical role of coupled electron/proton tunneling in the mechanism of this particular reaction. The discovery that Mo nitrogenase is capable of using CO as a substrate, albeit at a considerably lower rate than its V counterpart, more broadly supports the hypothesis that CO reduction is an evolutionary relic of the function of this enzyme family. The parallelism between the nitrogenase-catalyzed CO and N_2 reduction—demonstrated further by the ability of V nitrogenase to form CH_4, an analogous product of NH_3—strengthens the theory that the ancestral nitrogenase may represent an evolutionary link between carbon and nitrogen cycles on earth (*7*). In a practical vein, the industrial Fischer-Tropsch process uses H_2, a costly syngas component, for CO reduction and shows a tendency toward excessive formation of CH_4, a low-value product (*17*), whereas the nitrogenase-based reaction uses H^+ for hydrocarbon formation and favors the formation of C-C bond over the cleavage of C-O bond. These features make nitrogenase an attractive template for cost-efficient hydrocarbon formation that is directed toward C-C coupling and carbon-chain extension. Borrowing a trick or two from this ancient enzyme family, perhaps an efficient strategy could be developed in the future for controlled fuel production from CO? Only time will tell.

References and Notes

1. B. K. Burgess, D. J. Lowe, *Chem. Rev.* **96**, 2983 (1996).
2. B. J. Hales, *Adv. Inorg. Biochem.* **8**, 165 (1990).
3. H. Schindelin, C. Kisker, J. L. Schlessman, J. B. Howard, D. C. Rees, *Nature* **387**, 370 (1997).
4. C. C. Lee, Y. Hu, M. W. Ribbe, *Proc. Natl. Acad. Sci. U.S.A.* **106**, 9209 (2009).
5. A small-scale nitrogenase reaction typically features 0.15 mg VFe or MoFe protein, the catalytic component of V or Mo nitrogenase. Such an assay condition was established empirically some 30 years ago (*6*) and has since been used as the conventional scale of in vitro nitrogenase assays in the field.
6. B. K. Burgess, D. B. Jacobs, E. I. Stiefel, *Biochim. Biophys. Acta* **614**, 196 (1980).
7. C. C. Lee, Y. Hu, M. W. Ribbe, *Science* **329**, 642 (2010).
8. Based on the retention time on a gas chromatograph column, the low–molecular-weight hydrocarbon products formed by the $Val^{\alpha 70}$-substituted Mo nitrogenase variants have been assigned as methane, ethylene, ethane, propylene, and propane (*9*).
9. Z. Y. Yang, D. R. Dean, L. C. Seefeldt, *J. Biol. Chem.* **286**, 19417 (2011).
10. C. K. Rofer-DePoorter, *Chem. Rev.* **81**, 447 (1981).
11. C. C. Lee, Y. Hu, M. W. Ribbe, *Angew. Chem. Int. Ed. Engl.* **50**, 5545 (2011).
12. Materials and methods are available as supporting material on *Science* Online.
13. Given the detection threshold of CH_4 (0.0007 nmol per nmol protein per min) and the activity of V nitrogenase in CH_4 production (0.12 nmol per nmol protein per min), the Mo nitrogenase is at least 170-fold less active than its V counterpart in catalyzing the formation of CH_4 from CO.
14. Only 0.04% of electrons can be traced in the hydrocarbon products formed in the Mo nitrogenase–catalyzed reaction.
15. E. C. Carnahan, J. D. Protasiewicz, S. J. Lippard, *Acc. Chem. Res.* **26**, 90 (1993).
16. The effect of deuterium on nitrogenase-catalyzed CO reduction is probably multifaceted. Apart from the inverse kinetic isotope effects (i.e., $k_H/k_D < 1$, where k_H and k_D are the rate constants of H_2O- and D_2O-based reactions, respectively) of D_2O that favor the formation of deuterated products (*18*, *19*), other solvent effects of D_2O—such as those affecting the protein conformation, the interaction between proteins, and the network of hydrogen bonds—have been observed (*20*–*23*).
17. A. A. Khodadadi, R. R. Hudgins, P. L. Silveston, *Can. J. Chem. Eng.* **74**, 695 (1996).
18. K. A. Kurtz, P. F. Fitzpatrick, *J. Am. Chem. Soc.* **119**, 1155 (1997).
19. D. G. Churchill, K. E. Janak, J. S. Wittenberg, G. Parkin, *J. Am. Chem. Soc.* **125**, 1403 (2003).
20. W. E. Karsten, C. J. Lai, P. F. Cook, *J. Am. Chem. Soc.* **117**, 5914 (1995).
21. T. V. Morgan *et al.*, *Biochemistry* **29**, 3077 (1990).
22. M. Cassman, *Arch. Biochem. Biophys.* **165**, 60 (1974).
23. S. Y. Sheu, E. W. Schlag, H. L. Selzle, D. Y. Yang, *J. Phys. Chem. A* **112**, 797 (2008).

Acknowledgments: We thank D. C. Rees and N. Dalleska of the California Institute of Technology (Pasadena, CA) for help with the GC-MS analysis. This work was supported by Herman Frasch Foundation grant 617-HF07 (M.W.R.) and NIH grant GM 67626 (M.W.R.).

Supporting Online Material

www.sciencemag.org/cgi/content/full/333/6043/753/DC1
Materials and Methods
Figs. S1 to S4
Table S1
References (*24*, *25*)

12 April 2011; accepted 16 June 2011
10.1126/science.1206883

High-Speed Atomic Force Microscopy Reveals Rotary Catalysis of Rotorless F_1-ATPase

Takayuki Uchihashi,[1,2,3]* Ryota Iino,[3,4,5]* Toshio Ando,[1,2,3]† Hiroyuki Noji[3,4,5]†

F_1 is an adenosine triphosphate (ATP)–driven motor in which three torque-generating β subunits in the $\alpha_3\beta_3$ stator ring sequentially undergo conformational changes upon ATP hydrolysis to rotate the central shaft γ unidirectionally. Although extensive experimental and theoretical work has been done, the structural basis of cooperative torque generation to realize the unidirectional rotation remains elusive. We used high-speed atomic force microscopy to show that the rotorless F_1 still "rotates"; in the isolated $\alpha_3\beta_3$ stator ring, the three β subunits cyclically propagate conformational states in the counterclockwise direction, similar to the rotary shaft rotation in F_1. The structural basis of unidirectionality is programmed in the stator ring. These findings have implications for cooperative interplay between subunits in other hexameric ATPases.

F_1-ATPase, a water-soluble portion of adenosine triphosphate (ATP) synthase (*1*), is a rotary motor protein. The $\alpha_3\beta_3\gamma$ subcomplex (referred to here as F_1) suffices as the motor, in which the rotor γ subunit rotates in the stator $\alpha_3\beta_3$ ring upon ATP hydrolysis (*2*). The concept of the "rotary catalysis" of F_1 was proposed on the basis of biochemical studies (*3*). It was strongly supported by the first crystal structure reported (*4*) and directly proven by observations of rotating single molecules (*5*). In F_1, the catalytic sites are located at the α-β interfaces, mainly on the β subunits. In the crystal structure (*4*), three catalytic sites are in different nucleotide-bound states; one binds to an ATP analog (α_{TP}-β_{TP} in Fig. 1E), another binds to adenosine diphosphate (ADP) (α_{DP}-β_{DP}), and the third is unbound (α_E-β_E). Both β_{TP} and β_{DP} assume the closed conformation, swinging the C-terminal domain toward γ, whereas β_E assumes the open conformation, swinging the domain away from γ. Because these two general conformational states appear to push or be pushed by γ, respectively, it was proposed that interactions with γ control the conformational and catalytic states of individual β's to sequentially generate torque (*6*). In fact, some biochemical studies are thought to suggest that the $\alpha_3\beta_3$ ring alone does not possess intrinsic cooperativity, and γ mediates the interplay among β's (*7*–*9*). This view was reinforced by studies showing that backward mechanical rotation of γ with external force reverses the chemical reaction toward ATP synthesis (*10*, *11*), whereas forced forward rotation results in accelerated ATP binding (*12*).

[1]Department of Physics, Kanazawa University, Kakuma-machi, Kanazawa 920-1192, Japan. [2]Bio–AFM Frontier Research Center, College of Science & Engineering, Kanazawa University, Kakuma-machi, Kanazawa 920-1192, Japan. [3]Core Research for Evolutional Science and Technology, Japan Science and Technology Agency, Sanban-cho, Chiyoda-ku, Tokyo 102-0075, Japan. [4]Institute of Scientific and Industrial Research, Osaka University, Ibaraki, Osaka 567-0047, Japan. [5]Department of Applied Chemistry, School of Engineering, The University of Tokyo, Bunkyo-ku, Tokyo 113-8656, Japan.

*These authors contributed equally to this work.
†To whom correspondence should be addressed. E-mail: hnoji@appchem.t.u-tokyo.ac.jp (H.N.); tando@staff.kanazawa-u.ac.jp (T.A.)

Recently, however, this contention has been challenged by the finding that even when most interaction sites between β and γ are abolished, F_1 retains catalytic power to rotate γ unidirectionally (*13*, *14*). A few biochemical studies also suggest the intrinsic cooperativity of the $\alpha_3\beta_3$ ring (*15*, *16*). However, because conventional single-molecule optical microscopy requires attachment of a probe onto the rotary shaft for visualization (*5*), it does not allow direct examination of whether the intrinsic cooperativity in the $\alpha_3\beta_3$ ring is the core feature responsible for sequential torque generation. We clarified this issue by directly imaging the ATP-driven conformational transition of β's in the isolated $\alpha_3\beta_3$ ring, using high-speed atomic force microscopy (AFM) (*17*, *18*), a technique that can visualize proteins at work in real time without probes (*19*, *20*).

The $\alpha_3\beta_3$ subcomplex (fig. S1) was covalently immobilized on a mica surface and observed with high-speed AFM with a frame capture time of 80 ms unless otherwise mentioned (Fig. 1 and figs. S2 and S3). In the absence of nucleotide, the $\alpha_3\beta_3$ showed a pseudo-sixfold symmetric ring in which three alternately arranged subunits were elevated relative to the other three (Fig. 1A and fig. S4). The simulated AFM image of the C-terminus side of the ring constructed from the crystal structure of the nucleotide-free $\alpha_3\beta_3$ subcomplex (*21*) well reproduced the observed image (Fig. 1C). This indicates that the N-terminus side was selectively attached to the mica, although a smaller ring corresponding to the N-terminus side was occasionally observed (fig. S5). The three β's, which all assumed an open conformation in the crystal structure of $\alpha_3\beta_3$, gave three protruding peaks in the simulated image as bright spots. When a nonhydrolyzable ATP analog AMPPNP was added, the ring became triangular and the central hole was obscured (Fig. 1D). Although the three α's with lower protrusions retained the same conformation as those under the nucleotide-free condition, two of three

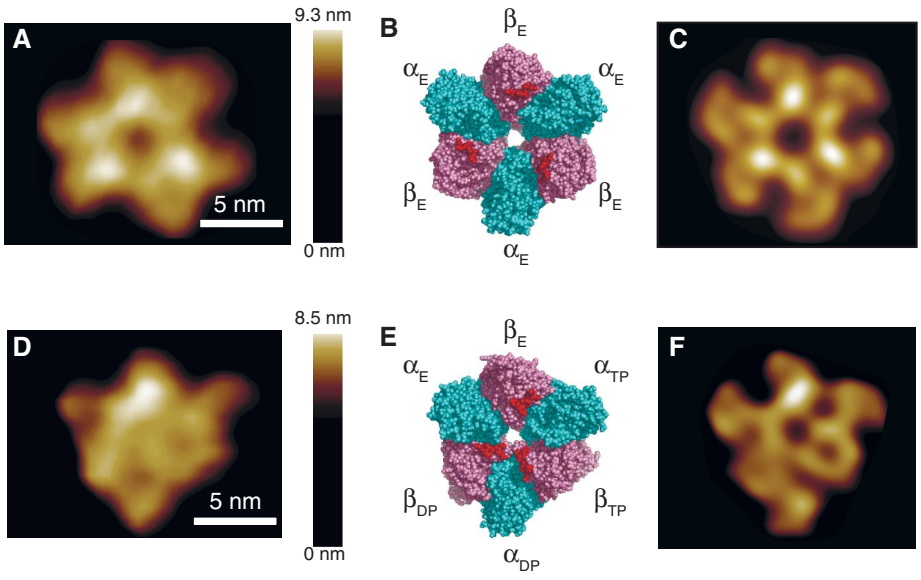

Fig. 1. (**A**) Averaged AFM image of C-terminal side of the $\alpha_3\beta_3$ subcomplex without nucleotide (movie S1). (**B**) C-terminal side of the crystal structure of the nucleotide-free $\alpha_3\beta_3$ subcomplex [Protein Data Bank (PDB) code 1SKY] (*21*). The α and β subunits are colored in cyan and pink, respectively. The C-terminal DELSEED motif of β corresponding to the high protruding portions is highlighted in red. (**C**) Simulated AFM image of the $\alpha_3\beta_3$ subcomplex constructed from the structure in (B). (**D**) Averaged AFM image of C-terminal side of the $\alpha_3\beta_3$ subcomplex in 1 mM AMPPNP. (**E**) Atomic structure of the $\alpha_3\beta_3$ subcomplex with bound nucleotides. This structure is obtained by removing γ from the crystal structure of F_1 (PDB code 1BMF) (*4*). (**F**) Simulated AFM image constructed from the structure in (E). The brightness of all AFM images in this paper represents the sample height but is not linearly set to highlight the top surface structure (fig. S4).

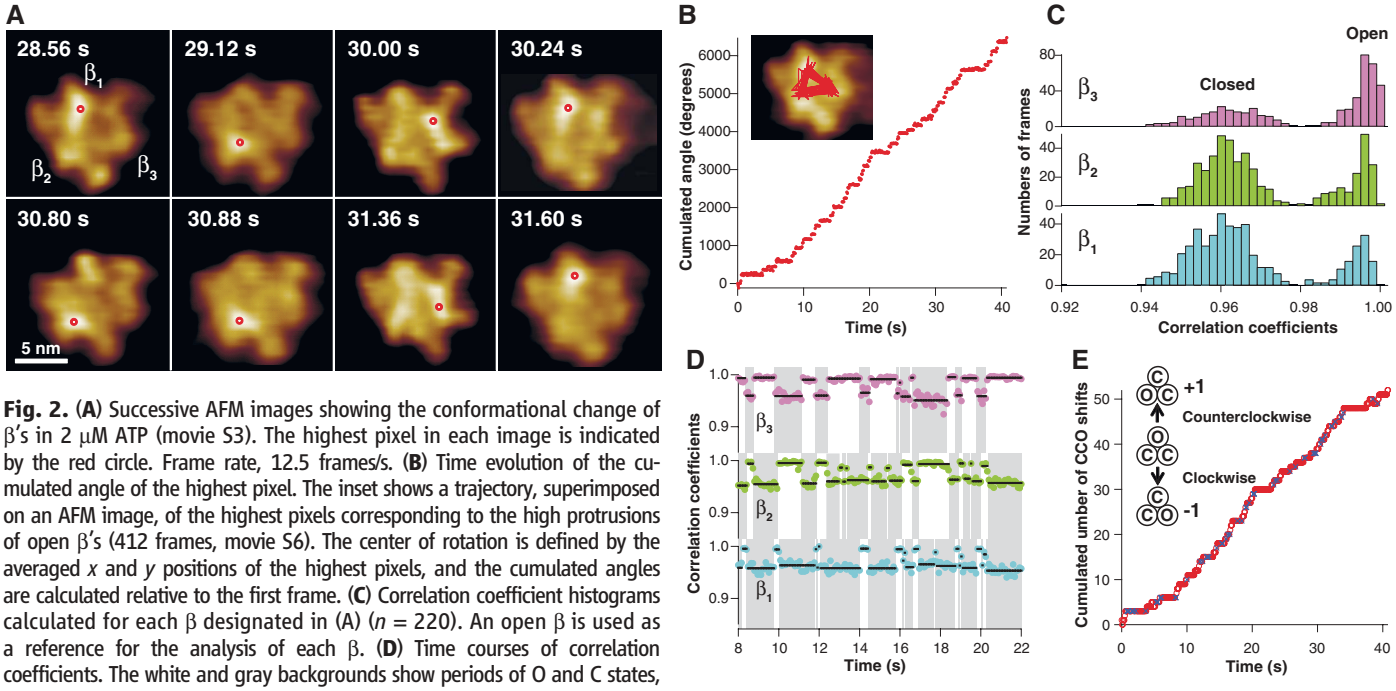

Fig. 2. (**A**) Successive AFM images showing the conformational change of β's in 2 μM ATP (movie S3). The highest pixel in each image is indicated by the red circle. Frame rate, 12.5 frames/s. (**B**) Time evolution of the cumulated angle of the highest pixel. The inset shows a trajectory, superimposed on an AFM image, of the highest pixels corresponding to the high protrusions of open β's (412 frames, movie S6). The center of rotation is defined by the averaged *x* and *y* positions of the highest pixels, and the cumulated angles are calculated relative to the first frame. (**C**) Correlation coefficient histograms calculated for each β designated in (A) (n = 220). An open β is used as a reference for the analysis of each β. (**D**) Time courses of correlation coefficients. The white and gray backgrounds show periods of O and C states, respectively. Solid lines show the mean correlation coefficient for each period. (**E**) Time evolution of the cumulated number of counterclockwise shifts of the CCO state. Circles, x's, and crosses correspond to CCO, COO, and other irregular states (OOO and CCC), respectively. The increase in the cumulated number indicates that the open β in CCO shifts counterclockwise.

β's retracted toward the center and simultaneously lowered their protrusions. Consequently, the ring showed a single high protrusion. A simulated image of $\alpha_3\beta_3$ with bound nucleotides was constructed using a structure in which γ was removed from the crystal structure of F_1 (Fig. 1E) (*4*). The simulated image (Fig. 1F) also showed an asymmetric ring very similar to that of the observed image. The excellent agreement indicates that only two β's can assume the closed conformation, even in saturating AMPPNP. This feature is consistent with the observation that three β's do not assume the closed conformation simultaneously (*22*).

When ATP was added, β showed distinct conformational dynamics; each β underwent a conformational transition between the outwardly extended high state (open) and the retracted low state (closed) (Fig. 2A and table S1); the outwardly extended and retracted conformations correlated well with the high- and low-protrusion states, respectively (fig. S6). The most prominent features are that only a single β assumes the open state, as in the presence of AMPPNP, and that when the open-to-closed transition occurs at one β, the opposite closed-to-open transition occurs simultaneously at its counterclockwise neighbor β in most cases. Thus, the high and outwardly extended conformation propagates in the counterclockwise direction (Fig. 2, A and B).

For a more quantitative analysis of this cooperativity, the conformational states of the three β's in each image frame were determined from their correlation coefficients, using respective reference images of β's in the open state (fig. S7). The correlation coefficients are distributed around two distinct peaks at ~0.995 and ~0.96 (Fig. 2C). The peaks with larger and smaller coefficients correspond to the open (O) and closed (C) states, respectively. On the other hand, the correlation coefficient analysis for the nucleotide-free and AMPPNP-bound $\alpha_3\beta_3$ showed static conformations of β (figs. S8 and S9 and table S1). Figure 2D shows typical time courses of the two conformational states for individual β's. In all images observed in the presence of 2 to 4 μM ATP (n = 8746 frames), three β's at a given frame dominantly showed the CCO state (82% of total). The COO state was also observed (14.5%). Other states such as CCC (3%) and OOO (0.5%) were rare. We analyzed the rotary propagation of the O and C states by counting the number of counterclockwise shifts of the CCO state [Fig. 2E and supporting online material (SOM)]. The propagation is unidirectional, rotating counterclockwise with an efficiency of 83% (in 2 μM ATP) over the total shift events examined (n = 371) (fig. S10). Considering that two consecutive counterclockwise shifts occurring occasionally within the frame capture time (80 ms) would be counted as a clockwise shift, this value of efficiency is probably underestimated by ~6% (Fig. 3D, fig. S11, and SOM).

The rate of rotational propagation of the CCO state increased with increasing ATP concentration (Fig. 3, A to C), indicating that ATP binding is rate-limiting, consistent with the biochemically determined Michaelis constant of 12 μM for ATP hydrolysis (fig. S1). Histograms of the dwell time of the O state followed a single exponential function, and those of the C state were well fitted with the model that two consecutive events of ATP binding to the other two β's trigger the transition of the β from the C to the O state (fig. S11). The rate constants of the counterclockwise shift of the CCO state were comparable with the initial rates of ATP hydrolysis measured biochemically (Fig. 3D). Thus, each ATP hydrolysis is well coupled with the open-to-closed transition of β. Just before transitioning to the next CCO state, a COO state occasionally appeared (~30% of total transitions) (x's in Figs. 2E and 3, A to C). In this event, one of the two closed β's positioned at the counterclockwise side opened in most cases, implying that ADP can be released from the closed β before ATP binds to the open β (*23*, *24*).

The present results prove that the stator $\alpha_3\beta_3$ ring alone possesses high cooperativity for sequential power stroking among three catalytic β's. This was also indicated by the observations that the occasional subunit dissociation completely stopped the rotary propagation of the conformational state (fig. S12). Thus, the "γ-dictator" model (*13*), which proposes that only the interaction with γ determines the conformational and catalytic states of β's (*23*, *24*), is not valid. On the other hand, the ATP-binding rate and the efficiency of unidirectionality of the $\alpha_3\beta_3$ subcomplex are distinctly lower than those of F_1 (Fig. 3 and fig. S11). Thus, the interaction with γ is dispensable but still important for the rapid and precise rotary catalysis. Our findings are not inconsistent with the observations that the rates and equilibriums of the catalytic reactions are apparently under the control of the rotary angle of γ (*10*–*12*). The intrinsic interplay among β's would reinforce catalytic control by γ; even if γ tightly interacts with only one β, it still can act on all β's through β-β interplay.

These results also have implications for the cooperativity of other structurally related hexameric ATPases such as RecA- and AAA+-family proteins, in which cooperativity among the separate catalytic sites is a central issue (*25*). These ATPases may also have intrinsic cooperativity. Comparative studies on these proteins should shed light on the common operating principles of hexameric ATPases.

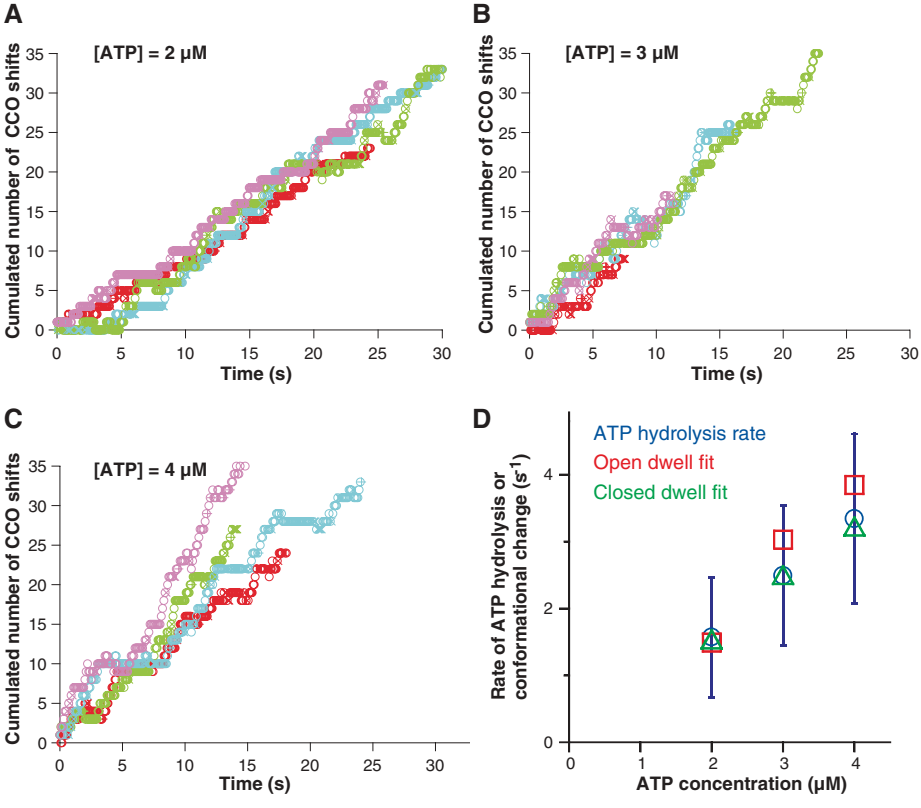

Fig. 3. (**A** to **C**) Time evolutions of the cumulated number of counterclockwise CCO shifts at various concentrations of ATP ([ATP]). At each [ATP], four representative curves for the different molecules are indicated as in Fig. 2E. (**D**) [ATP] dependence of the initial rates of ATP hydrolysis determined by biochemical assay [circles; 2 μM, 1.6 ± 0.9 s^{-1}; 3 μM, 2.5 ± 1.0 s^{-1}; 4 μM, 3.3 ± 1.3 s^{-1} (mean ± SD, n = 6 individual measurements at each [ATP])] and the rates of conformational change of β determined by fitting the dwell time histograms of open (squares; 2 μM, 1.5 s^{-1}; 3 μM, 3.0 s^{-1}; 4 μM, 3.8 s^{-1}) and closed (triangles; 2 μM, 1.5 s^{-1}; 3 μM, 2.5 s^{-1}; 4 μM, 3.2 s^{-1}) states shown in fig. S11.

References and Notes

1. P. D. Boyer, *Annu. Rev. Biochem.* **66**, 717 (1997).
2. W. Junge, H. Sielaff, S. Engelbrecht, *Nature* **459**, 364 (2009).
3. M. J. Gresser, J. A. Myers, P. D. Boyer, *J. Biol. Chem.* **257**, 12030 (1982).
4. J. P. Abrahams, A. G. Leslie, R. Lutter, J. E. Walker, *Nature* **370**, 621 (1994).
5. H. Noji, R. Yasuda, M. Yoshida, K. Kinosita Jr., *Nature* **386**, 299 (1997).
6. H. Wang, G. Oster, *Nature* **396**, 279 (1998).
7. C. Kaibara, T. Matsui, T. Hisabori, M. Yoshida, *J. Biol. Chem.* **271**, 2433 (1996).
8. J. J. García, R. A. Capaldi, *J. Biol. Chem.* **273**, 15940 (1998).
9. R. K. Nakamoto, C. J. Ketchum, M. K. al-Shawi, *Annu. Rev. Biophys. Biomol. Struct.* **28**, 205 (1999).
10. H. Itoh *et al.*, *Nature* **427**, 465 (2004).
11. Y. Rondelez *et al.*, *Nature* **433**, 773 (2005).
12. Y. Iko, K. V. Tabata, S. Sakakihara, T. Nakashima, H. Noji, *FEBS Lett.* **583**, 3187 (2009).
13. S. Furuike *et al.*, *Science* **319**, 955 (2008).
14. N. Mnatsakanyan, A. M. Krishnakumar, T. Suzuki, J. Weber, *J. Biol. Chem.* **284**, 11336 (2009).
15. M. Yoshida, W. S. Allison, *J. Biol. Chem.* **265**, 2483 (1990).
16. P. Aloise, Y. Kagawa, P. S. Coleman, *J. Biol. Chem.* **266**, 10368 (1991).
17. T. Ando *et al.*, *Proc. Natl. Acad. Sci. U.S.A.* **98**, 12468 (2001).
18. T. Ando, T. Uchihashi, T. Fukuma, *Prog. Surf. Sci.* **83**, 337 (2008).
19. M. Shibata, H. Yamashita, T. Uchihashi, H. Kandori, T. Ando, *Nat. Nanotechnol.* **5**, 208 (2010).
20. N. Kodera, D. Yamamoto, R. Ishikawa, T. Ando, *Nature* **468**, 72 (2010).
21. Y. Shirakihara *et al.*, *Structure* **5**, 825 (1997).
22. R. I. Menz, J. E. Walker, A. G. Leslie, *Cell* **106**, 331 (2001).
23. K. Adachi *et al.*, *Cell* **130**, 309 (2007).
24. R. Watanabe, R. Iino, H. Noji, *Nat. Chem. Biol.* **6**, 814 (2010).
25. E. J. Enemark, L. Joshua-Tor, *Curr. Opin. Struct. Biol.* **18**, 243 (2008).

Acknowledgments: We thank M. Tanigawara, H. Yamashita, R. Hasegawa, and D. Okuno for technical help and members of the Noji and Ando laboratories for valuable comments. This work was supported by Grants-in-aid for Scientific Research from the Ministry of Education, Culture, Sports, Science and Technology project ID nos. 18074005, 18201025, 21770168, 21681017, 2102301, 21107517, 22247025, and 20221006); the Knowledge Cluster Initiative; and the Japan Science and Technology Agency for Core Research for Evolutional Science and Technology.

Supporting Online Material

www.sciencemag.org/cgi/content/full/333/6043/755/DC1
Materials and Methods
Figs. S1 to S12
Table S1
References (*26*–*28*)
Movies S1 to S8

11 March 2011; accepted 21 June 2011
10.1126/science.1205510

Structural Basis for Tail-Anchored Membrane Protein Biogenesis by the Get3-Receptor Complex

Susanne Stefer,[1]* Simon Reitz,[2]* Fei Wang,[3] Klemens Wild,[2] Yin-Yuin Pang,[2] Daniel Schwarz,[4] Jörg Bomke,[4] Christopher Hein,[1] Frank Löhr,[1] Frank Bernhard,[1] Vladimir Denic,[3]† Volker Dötsch,[1]† Irmgard Sinning[2]†

Tail-anchored (TA) proteins are involved in cellular processes including trafficking, degradation, and apoptosis. They contain a C-terminal membrane anchor and are posttranslationally delivered to the endoplasmic reticulum (ER) membrane by the Get3 adenosine triphosphatase interacting with the hetero-oligomeric Get1/2 receptor. We have determined crystal structures of Get3 in complex with the cytosolic domains of Get1 and Get2 in different functional states at 3.0, 3.2, and 4.6 angstrom resolution. The structural data, together with biochemical experiments, show that Get1 and Get2 use adjacent, partially overlapping binding sites and that both can bind simultaneously to Get3. Docking to the Get1/2 complex allows for conformational changes in Get3 that are required for TA protein insertion. These data suggest a molecular mechanism for nucleotide-regulated delivery of TA proteins.

Sophisticated mechanisms have evolved to target eukaryotic membrane proteins to the correct membrane-surrounded organelle and to protect them from aggregation. Of central importance are cytosolic factors that decode the targeting information of a signal sequence by transient association and escort membrane proteins to their designated location (*1*, *2*). Tail-anchored membrane proteins (TA proteins) consist of a N-terminal soluble domain and a single C-terminal transmembrane domain (TMD) (*3*–*5*). The C-terminal localization of their targeting signal requires release of the synthesized protein from the ribosome before interaction with an insertion machinery (*6*). This precludes TA proteins from cotranslational insertion mediated by the signal recognition particle (SRP)–Sec61 translocon system (*7*–*9*), which mainly targets membrane proteins with a N-terminal signal sequence. Although some studies suggest an unassisted insertion of TA proteins into the mitochondrial outer membrane (*10*, *11*), most endoplasmic reticulum (ER)–destined TA proteins are thought to insert by an energy-dependent process, which involves several cytosolic factors (*2*, *12*–*17*). In yeast, it was shown that the adenosine triphosphatase (ATPase) Get3 is necessary for the biogenesis of TA proteins (*2*, *18*). Get3 is a dimeric protein with each subunit comprising a nucleotide-binding domain (NBD) and a methionine-rich α-helical domain that has been implicated in TA protein binding (TA binding domain, TABD). Crystal structures of Get3 have shown that the protein switches between an open and closed state, depending on its nucleotide load. Whereas in the apo and magnesium-free adenosine diphosphate (ADP) forms the open state is favored (*19*–*23*), ADP-Mg^{2+} and the nonhydrolyzable ATP analog 5′-adenylyl-β,γ-imidodiphosphate–Mg^{2+} (AMPPNP-Mg^{2+}) induce the closed state (*19*), which is further tightened up in the transition state of adenosine triphosphate (ATP) hydrolysis (*20*). The hydrophobic groove responsible for TA binding seems fully assembled only in the transition state (*20*). At the membrane, Get3 interacts with the two receptor proteins, Get1 and Get2, which are essential for TA protein insertion (*2*). In order to understand the molecular mechanisms underlying Get3-dependent membrane insertion of TA proteins, we determined crystal structures of Get3 in complex with the soluble domains of its membrane-bound Get1 and Get2 receptors and functionally characterized the interaction in different nucleotide-bound states.

Get1 and Get2 are integral membrane proteins, and each comprises three TMDs (Fig. 1A). In order to analyze the Get3-receptor interaction in more detail, we performed flotation assays of Get3 with microsomal membranes (RMs) (Fig. 1B) and insertion assays with the TA protein Sec22 [a soluble *N*-ethylmaleimide–sensitive factor attachment protein receptor (SNARE) protein] in the presence of different nucleotides (Fig. 1C) (*2*, *14*, *15*). Efficient TA protein insertion was observed in presence of ATP and ADP, but not with adenosine 5′-*O*-(3-thiotriphosphate) (ATP-γ-S)—in line with Get3 recruitment observed in the flotation assays. Get1-CD (residues 19 to 103) is the most conserved region of Get1 and predicted to adopt a coiled-coil structure (*24*) with two long helices (α1 and α2) extending the flanking transmembrane regions (Fig. 1A and fig. S1A), similar to its human homolog, the tryptophan-rich basic protein, WRB (*25*, *26*). Using a pull-down approach, we found that detergent-solubilized Get1 efficiently binds to Get3 (fig. S2A). Additional truncation constructs

[1]Institute for Biophysical Chemistry, Centre for Biomolecular Magnetic Resonance, Goethe University, D-60325 Frankfurt am Main, Germany. [2]Heidelberg University Biochemistry Center (BZH), Im Neuenheimer Feld 328, D-69120 Heidelberg, Germany. [3]Department of Molecular and Cellular Biology, Harvard University, Northwest Laboratories, Cambridge, MA 02138, USA. [4]Merck KGaA, Merck Serono, Molecular Interactions and Biophysics, D-64293 Darmstadt, Germany.

*These authors contributed equally to this work.
†To whom correspondence should be addressed. E-mail: irmi.sinning@bzh.uni-heidelberg.de (I.S.); vdoetsch@em.uni-frankfurt.de (V.D.); vdenic@mcb.harvard.edu (V.D.)